HIV-1 Nucleocapsid Protein NCp7 and Its RNA Stem Loop 3 Partner: Rotational Dynamics of Spin-Labeled RNA Stem Loop 3[†]

Xiangmei Xi,[‡] Yan Sun,[‡] Christine B. Karim,[§] Vladimir M. Grigoryants,[‡] and Charles P. Scholes*[,‡]

Department of Chemistry, University at Albany—SUNY, Albany, New York 12222, and Department of Biochemistry, Molecular Biology and Biophysics, University of Minnesota, Minneapolis, Minnesota 55455

Received April 5, 2008; Revised Manuscript Received June 27, 2008

ABSTRACT: The tumbling dynamics of a 20-mer HIV-1 RNA stem loop 3 spin-labeled at the 5′ position were probed in the nanosecond time range. This RNA interacted with the HIV-1 nucleocapsid Zn-finger protein, 1−55 NCp7, and specialized stopped-flow EPR revealed concomitant kinetics of probe immobilization from milliseconds to seconds. RNA stem loop 3 is highly conserved in HIV, while NCp7 is critical to HIV-RNA packaging and annealing. The 5′ probe did not perturb RNA melting or the NCp7/RNA interaction monitored by gel shift and fluorescence. The 5′-labeled RNA tumbled with a subnanosecond isotropic correlation time (∼0.60 ns at room temperature) reflecting both local viscosity-independent bond rotation of the probe and viscosity-dependent diffusion of 40−60% of the RNA. The binding of NCp7 to spin-labeled RNA stem loop 3 in a 1:1 ratio increased the spin-labeled tumbling time by about 40%. At low ionic strength with a ratio of NCp7 to RNA ≥3 (i.e., an NCp7 to nucleotide ratio ≤7, which is the threshold ratio for chaperone effects), the probe tumbling time markedly increased to several nanoseconds, signifying a NCP7/RNA complex with restricted motion even at the initially mobile 5′ position. Increasing the ionic strength to shield the electrostatic attraction between polyanionic RNA and polycationic NCp7 eliminated this immobilization. Forming the immobilized ≥3:1 complex also required intact Zn fingers. Stopped-flow EPR kinetics with NCP7/RNA mixed at a 4:1 ratio showed the major phase of NCp7 interaction with RNA stem loop 3 occurred within 4 ms, a second phase occurred with a time constant of ∼30 ms, and a slower immobilization, possibly concomitant with large complex formation, proceeded over seconds. This work points the way for spin-labeling to investigate oligonucleotide-protein complexes, notably those lacking precise stoichiometry, that are requisite for viral packaging and genome fabrication.

The structure and function of the HIV-1 nucleocapsid protein, NCp7, have been studied through its interaction with the four contiguous stem loop structures, SL1−SL4 of the HIV-1 Ψ recognition site (*1*−*4*). Figure 1 shows the RNA stem loop 3 (*5*) combining with the relatively unstructured NCp7 Zn-finger protein (*6*) to form a 1:1 RNA-protein complex (*1*), and Scheme 1 shows the nucleotide sequence of the 6.5 kDa 20-mer RNA stem loop 3 and the amino acid sequence of the 6.4 kDa 55-mer NCp7. RNA stem loop 3 is of particular interest because its sequence is highly conserved among different strains of HIV-1. A 1:1 complex, such as that shown by the NMR structure in Figure 1, provides useful structural information on specific binding of NCp7 to a stem loop RNA.

Although specific binding of NCp7 to secondary loop regions is an essential aspect of NCp7/RNA recognition, the overall coverage of the viral genome by NCp7 through processes beyond specific binding is important to the packaging-annealing process. The annealing process is important in the viral life cycle to facilitate the reverse transcription process of converting single strand genomic viral RNA to DNA for integration into the host and during maturation in packaging and protecting the genome from nucleases. The necessity for a nucleic acid chaperone arises because complementary strands of DNA or RNA are prevented from forming desirable duplexes when their individual single strands contain internal, self-pairing, stable

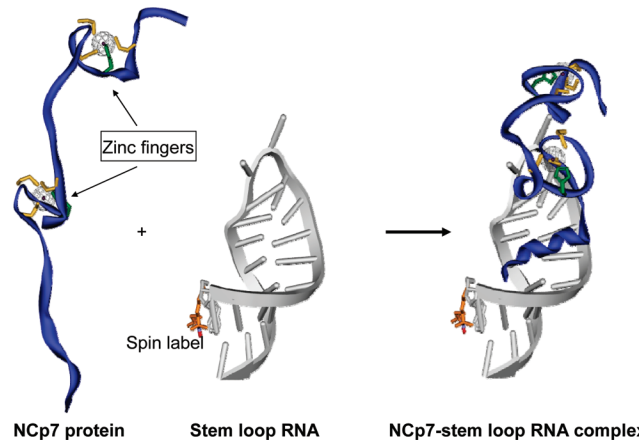

FIGURE 1: Ribbon diagrams showing the relatively unstructured NCp7 Zn-finger protein (*6*) combining with RNA stem loop 3 (*5*) to form a 1:1 RNA-protein complex (*1*).

[†] This work supported by the NIH (Grant GM066253-01A1 to C.P.S.) and the Minnesota Medical Foundation (MMF Grant to C.B.K.).

* Corresponding author. Telephone: 518-442-4551. Fax: 518-442-3462. E-mail: cps14@albany.edu.

[‡] University at Albany.

[§] University of Minnesota.

10.1021/bi800602e CCC: $40.75
Published on Web 08/26/2008

Scheme 1: Sequences of the HIV-1 Nucleocapsid Protein and RNA Stem Loop 3 with Which It Interacts[a]

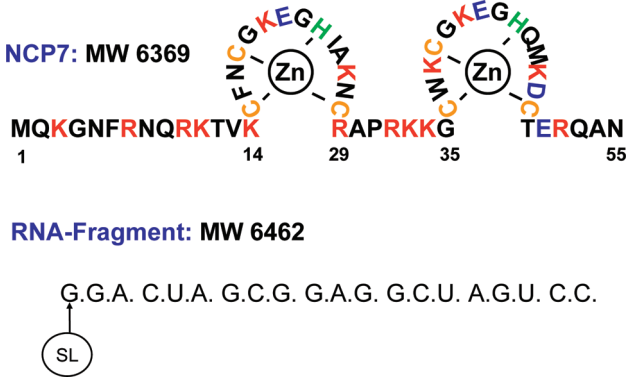

[a] "SL" indicates the end position where a spin-label is attached. Within the NCp7 sequence, red indicates positively charged basic residues. Orange indicates the cysteine residues within the Zn-finger structures. Blue indicates negatively charged acidic residues. Green indicates the histidine residues in each Zn-finger structure.

secondary regions, like the stems of stem loops. In the chaperone-annealing process, NCp7 molecules bind to these individual single strand oligonucleotides with some specific hydrogen bonding and hydrophobic affinity for the loop regions and less specific, electrostatically driven affinity for the stems. In binding to stem loop regions, the NCp7 molecules destabilize these stem loop structures and lower the activation energy barrier for the ultimate formation of stable duplex structures. The annealing process occurs with highest efficacy when the entire oligonucleotide is covered with NCp7 (*7*); that is, more than one NCp7 per oligonucleotide is required.

For labeling strategy, the literature for spin-labeling of RNA and RNA stem loop systems provides instances of labeling near the 5′ end (*8*−*10*) and within the RNA loop (*10, 11*). Recent work has focused on elaborating the dynamics at individual locations internal to RNA (*11*−*13*), at elaborating change in dynamics upon binding of other RNAs (*13*−*15*), of peptides (*8, 16, 17*), and of drugs (*16*), and in finding distance between labels (*13, 18*−*20*). To avoid perturbation of the loop region where the binding of NCp7 is most critical (Figure 1), our specific labeling strategy up to this point has been to monitor the motion of the RNA by a spin-label attached to the 5′ end position (Scheme 1), chosen not to impede specific stem loop-Zn-finger interactions.

Here we use EPR[1] to probe the structure and mobility of RNA stem loop 3 by itself and complexed with NCp7. (A corresponding paper focused on spin-labeled NCp7 has been accepted in *Biopolymers*.) The spin-label method has the advantage of sensing the nanosecond tumbling dynamics of the RNA and sensing how these dynamics are changed by NCp7 at various ratios. The spin-label does not require the highly structured macromolecular entities needed for NMR or crystallography. With specialized high sensitivity stopped-flow EPR (*21*−*23*), we obtain an additional picture showing how these nanosecond kinetics change as the spin-labeled RNA and the NCp7 recognize one another and form complexes on the millisecond and longer time scale.

[1] Abbreviations: EPR, electron paramagnetic resonance; CD, circular dichroism.

Scheme 2: Reaction of Iodoacetamide Spin-Label with Phosphorothioate Located at 5′G of Stem Loop RNA

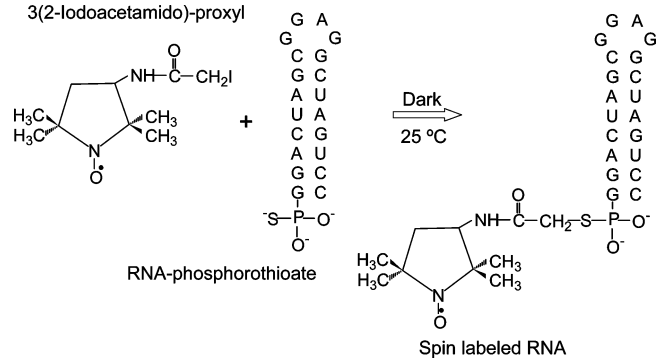

EXPERIMENTAL PROCEDURES

Preparation of Spin-Labeled RNA Stem Loop 3. In order to avoid perturbation of the RNA loop region, we have spin-labeled the RNA stem loop 3 by an iodoacetamide spin-label, which is attached at a 5′-phosphorothioate. The reaction is shown in Scheme 2. Macosko et al. (*8*) had previously end-labeled an RNA oligomer after incorporating a phosphorothioate at its 5′ terminal, and Ramos and Varani (*10*) had used the iodoacetamide spin-label to spin-label RNA.

5′-Phosphorothioate RNA (160 nmol) (Dharmacon, Inc.) was dissolved in 800 μL of 100 mM, pH 8.0, sodium phosphate buffer. 3-(2-Iodoacetamino)proxyl spin-label (5.2 mg) (Toronto Research Chemicals, North York, Ontario, Canada) was dissolved in 200 μL of 50% ethanol. This amount of spin-label provided a 100-fold mole ratio of spin probe to RNA. After mixing the spin-label with the 5′-phosphorothioate RNA, the reaction was allowed to proceed in the dark with continuous shaking for 20 h at room temperature. The RNA was extracted by 1-butanol (2 × 1.5 mL) and pooled to yield 200 μL of product solution. This product was loaded onto an NAP10 column to further separate the spin-labeled RNA from unreacted iodoacetamide spin probe, and gel purification was subsequently done.

Preparation of Nucleocapsid Protein NCp7. NCp7 was prepared by solid phase peptide synthesis with methods similar to those described previously (*24, 25*). The final NCp7 concentration of 2 mM was determined by using an extinction coefficient of $\epsilon_{280} = 6050\ M^{-1}\ cm^{-1}$ (*26*). Zinc chloride was added in a 2:1 molar ratio to NCp7, which was lyophilized and stored in liquid nitrogen.

Gel Characterization and Purification of Spin-Labeled RNA Stem Loop 3. Spin-label reaction products were purified using preparative PAGE and monitored using analytical PAGE. The protocols for preparative and analytical gel procedures are provided in the Supporting Information. Figure 2 provides an analytical gel showing the effectiveness of the spin-labeling protocol, as well as the existence of a dimer in the starting material. Lanes 4 and 5 of Figure 2 show gel-purified, spin-labeled RNA final product. Arrow 1 indicates a dimer which was contained in the 5′-phosphorothioate RNA starting material. Arrow 2 indicates the desired spin-labeled RNA stem loop 3. Arrow 3 indicates RNA stem loop 3 lacking the spin-label probe.

Molecular Mass Determination. The expected molecular mass of unlabeled RNA stem loop 3 is 6462 Da and of the spin-labeled RNA stem loop 3 is 6756 Da. The molecular masses determined by MALDI mass spectroscopy (using an

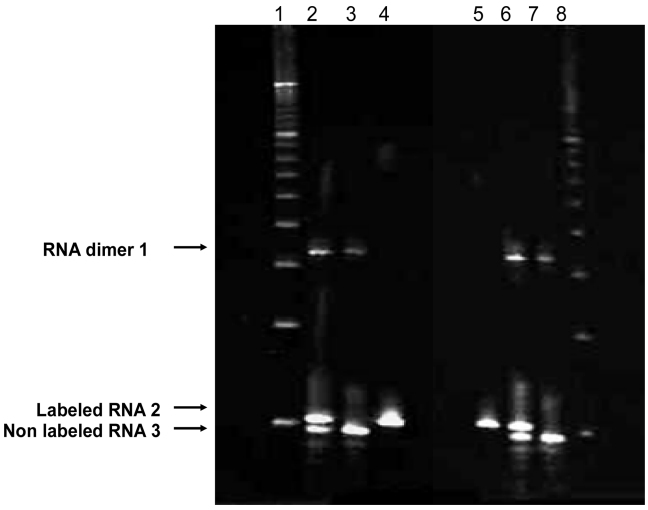

FIGURE 2: Denaturing PAGE gel showing RNA stem loop 3 bands before and after the spin-label reaction and gel purification. Lanes 1 and 8 are the DNA ladder where the lowest band is due to 20 bases, the next 30 bases, etc. Lanes 2 and 6 are the RNA spin-label reaction mixture. Lanes 3 and 7 are the 5′-phosphothiorate RNA starting material before the labeling reaction. Lanes 4 and 5 are the gel-purified, spin-labeled RNA.

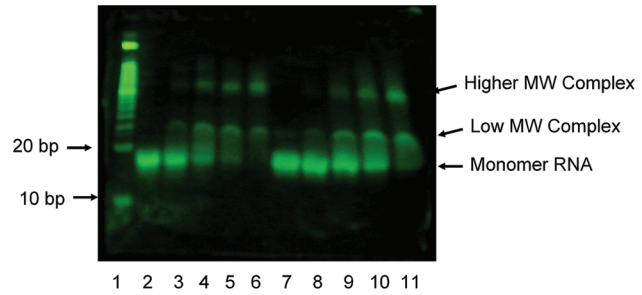

FIGURE 3: Gel retardation assay of RNA stem loop 3 in unlabeled form (lanes 2−6) and in spin-labeled form (lanes 7−11) in the presence of increasing amounts of NCp7. In these studies the concentration of the RNA stem loop 3 was approximately 1 μM in 50 mM Hepes buffer, pH 7.5, and the stain Sybergold (Molecular Probes) was used to detect the RNA subsequent to running the gel. Evidence for RNA stem loop 3-NCp7 complexes was observed thorough bands moving more slowly than RNA stem loop 3 by itself. Lane identifications are as follows: lane 1, DNA ladder; lane 2, unlabeled stem loop RNA; lanes 3−6, unlabeled stem loop RNA/NCP7 at ratios of 1:2, 1:4, 1:6, and 1:10; lane 7, labeled stem loop RNA; lanes 8−11, labeled stem loop RNA/NCP7 at ratios of 1:2, 1:4, 1:6, and 1:10.

Applied Biosystems Voyager System 1108) were 6460.94 Da for unlabeled RNA stem loop 3 and 6755.98 Da for the phosphorothioate spin-labeled RNA stem loop 3. (See mass spectra in Figure 1S, Supporting Information.)

NCp7/RNA Interaction Characterized by Nondenaturing Gel Shift Assay. Nondenaturing gel shift assays were run as shown in Figure 3 with the goal of providing a simple analytic comparison of the binding of spin-labeled RNA stem loop 3 and of unlabeled RNA stem loop 3 to NCp7 at various ratios of NCp7 to RNA stem loop 3. An overall comparison of the assay carried out with unlabeled RNA (Figure 3, lanes 2−6) to the assay carried out with labeled RNA (lanes 7−11) does provide the proof of the similarity in the NCp7 binding property of the unlabeled and the labeled RNA stem loop 3. The RNA by itself, either labeled or not, traveled fastest. At a ratio of 2:1 NCp7/RNA a complex started to appear, traveling slightly slower than the 30 bp marker which, in analogy with the 1:1 complex reported by Amarasinghe et al. (*4*) under similar gel conditions, could be a 1:1 complex. At ratios >2 of NCp7 to RNA stem loop 3, a more diffuse, more slowly moving, higher molecular mass complex appeared from which the stained intensity increased as the NCp7/RNA ratio increased. The existence of this last complex may imply that several NCp7 molecules may simultaneously bind to one RNA molecule. Previous gel retardation assays carried out with comparable conditions to those used with Figure 3 have also detected both 1:1 and 1:2 complexes of RNA stem loop 3 to NCp7 (*4*). Although we provide in this work EPR evidence for a complex at a 1:1 NCp7/RNA ratio and for higher order complexes, the conditions within the gel certainly differ from the solution conditions for EPR, and the concentrations of RNA and NCp7 for EPR are several orders of magnitude larger than those in the gel.

NCp7/RNA Interaction Characterized by Fluorescence Quenching of Trp37 in NCp7. The tryptophan residue at W37 is an internal NCp7 fluorophore whose fluorescence quenching permits titration of the interaction of NCp7 and provides another analytical method for comparison of spin-labeled and unlabeled RNA stem loop 3 (*2*). The fluorescence quenching titration was essentially identical for the unlabeled and spin-labeled RNA as shown in the Supporting Information, Figure 2SA. This quenching provided an experimental measure of the similarity in the binding of labeled and nonlabeled RNA stem loop 3 in binding NCp7. The fluorescence quenching, carried out at low ionic strength with submicromolar concentrations of RNA stem loop 3 and NCp7, indicated that several NCp7 can bind per RNA stem loop 3. We observed diminished fluorescence quenching, hence diminished binding, as the ionic strength was increased by increasing the NaCl concentration (Supporting Information, Figure 2SB).

UV−Vis Determination of RNA Melting. Melting of structured stem loop RNA is indicated by the hyperchromic effect in the 260−280 nm range. UV−vis data were collected and compared between labeled and unlabeled RNA stem loop 3 using a Varian 300 UV spectrometer equipped with a temperature controller. Melting indicated by the hyperchromic effect was recorded as a function of temperature at a ramp rate of 0.4 °C per minute from 20 to 95 °C. Fitting of the spectroscopic change to RNA melting behavior was performed using Tmelt (Texas A&M University (*27*)). The melting temperatures for labeled and unlabeled RNA were identical. In 20 mM, pH 7.5, Hepes the respective melting temperatures of unlabeled RNA stem loop 3 and spin-labeled RNA stem loop 3 were 76.8 and 76.6 °C. In 20 mM Hepes, 20 mM NaCl, and 0.2 mM $MgCl_2$ the melting temperatures were respectively 86.4 and 87.2 °C. The melting temperatures are thus unaltered by spin-labeling.

Analysis of Nucleocapsid Protein NCp7. Mass spectrometry (ESI-MS) was performed on the synthesized NCp7 in the positive ion mode using a Q Star (Applied Biosystems) instrument. The lyophilized NCp7 sample was dissolved in 70% acetonitrile/30% water/0.1% formic acid and diluted to a final concentration in the micromolar range. The deconvoluted mass spectra of the NCp7 showed one major peak at a molecular mass at 6369.00 Da, fully consistent with the calculated mass of 6369.05 Da.

SDS−PAGE was performed on the synthesized NCp7 using 10−20% Tris/Tricine gel (Bio-Rad). Sample loading

buffer (40 μL) (Bio-Rad) was added to the sample, which contained 5 μg of NCp7 in 50 mM Hepes, pH 7.5. NCp7 migrated as a monomer, moving slightly slower than phospholamban (PLB); the 6 kDa protein used as a reference (*25*).

EPR Spectroscopy. X-band (9.5 GHz) EPR spectra of spin-labeled RNA stem loop 3 were taken primarily at Albany at room temperature using a small, high sensitivity X-band dielectric resonator (DR) holding samples of approximately 1 μL volume (*21, 22, 28*). Microwave power of 0.64 mW (milliwatt) and modulation of about 1 G (gauss) were chosen so as not to broaden the EPR spectrum. Several samples were run at the University of Minnesota using the Bruker EleXsys 500 spectrometer.

The stopped-flow EPR system based on a rapid ball mixer intimately integrated to an X-band dielectric resonator (*21*−*23, 28*) was used for following the kinetic change in the spin-label signal of RNA stem loop 3 after mixing with NCp7.

EPR Line Shape Analysis for Estimation of Tumbling Correlation Times. Tumbling, as it modulates the anisotropic hyperfine and Zeeman interactions, causes the three hyperfine lines of the nitrogen $I = 1$ ^{14}N nucleus within the nitroxide spin-label to vary differently in amplitude and line width. As a spin-label becomes more mobile, there will be a relative increase in outer derivative ($M = \pm 1$) peak heights with respect to the central ($M = 0$) peak. [The peak heights between derivative extrema for these lines are taken as $h(+1)$, $h(0)$, and $h(-1)$.] When the tumbling correlation times are less than 1 ns, the times can be empirically estimated from these $h(+1)$, $h(0)$, and $h(-1)$ peak heights through analysis developed by Marsh (ref *29*, pp 259−262) and Miick et al. (*30*), which is outlined in the Supporting Information of Qu et al. (*31*).

EPR line shape simulations and correlation time determinations based on the stochastic Liouville equation were carried out using the nonlinear least-squares stochastic Liouville (NLSL) fitting programs developed by Freed and co-workers (*32*). These programs simulate the EPR line shape under conditions that need not be restricted to correlation times less than 1 ns. These simulations modeled the motion of the nitroxide by a rotational diffusion tensor, **R**. For isotropic diffusion $R_{iso} = 1/(6\tau_{iso})$, where τ_{iso} is the isotropic tumbling time. For axial anisotropic diffusion $R_{||} = 1/(6\tau_{||})$ and $R_{\perp} = 1/(6\tau_{\perp})$, where $\tau_{||}$ and $\tau_{\perp}$ are the corresponding anisotropic tumbling times. (Qin et al. (*14*) have provided an approximate expression for τ_{iso} when the tumbling is actually anisotropic, and it is $\tau_{iso} \approx (\tau_{\perp}\tau_{||})^{1/2}$.) In the present paper multiparameter NLSL fitting/simulation routines were used to provide estimates of the percentages of different sites within the same sample that had different correlation times. For the present samples a physical potential to restrict the motion of the spin-label (*33*) was not required and not statistically justified for fitting the EPR line shape.

RESULTS

Dynamics Reported by Spin-Labeled RNA Stem Loop 3 in the Absence of NCp7. The 5′ spin-label on RNA stem loop 3 indicated rapid subnanosecond tumbling, shown by the left-most spectrum in Figure 4, by the spectrum in Figure 6 in the absence of RNA, and by the simulation in Figure 3S, Supporting Information. The isotropic tumbling time, τ_{iso}, as estimated from the fitted simulation (*32*), was about 0.60 ns at room temperature, and the experimental EPR line shape was well simulated with an isotropic diffusion tensor.

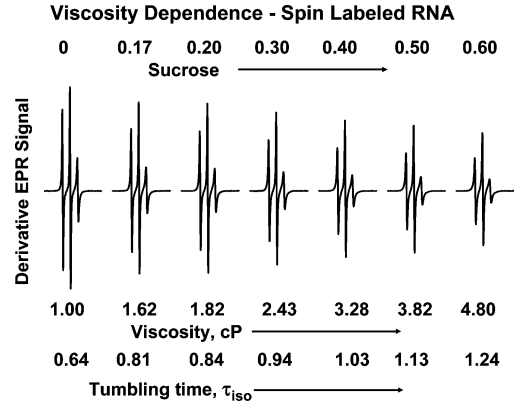

FIGURE 4: Derivative EPR spectra of 5′-labeled RNA stem loop 3 as a function of solvent viscosity in sucrose solution (g of sucrose/g of water) at 20 °C. Spectra were normalized by dividing by the second integral. Tumbling times were determined by fitting spectra to a single isotropic diffusion tensor (*32*).

It has been shown that spin-labels attached to RNA can report both fast local motions and slower viscosity-dependent motions (*14*). These two types of motion have been discriminated by monitoring the tumbling rate as a function of solvent viscosity (*14*). We varied solvent viscosity by varying the weight percent of sucrose (*34*), then we observed the systematically changing line shape, shown by the compendium of spectra in Figure 4, and then we estimated the correlation times, τ_{iso}.

Following Qin et al. (*14*), the measured tumbling rate $1/\tau_{iso}$ was approximated as the sum of a local viscosity-independent rate, $1/\tau_i$, and a viscosity-dependent rate, $1/(\eta\tau_R)$, where η is the true solvent viscosity in centipoise divided by the viscosity of water [$\eta = \eta/(\eta H_2O)$, where $\eta H_2O = 1$ cP].

$$1/\tau_{iso} = 1/\tau_i + 1/(\eta\tau_R) \quad (1)$$

τ_R has been explained as due to the motions of the RNA which experience viscous interaction with the solvent (*14*). (The Stokes−Einstein relation for an object tumbling in a viscous liquid indicates that the viscosity-dependent tumbling time τ_R should be proportional to the solvent viscosity and proportional to the volume of the tumbling object (*30*).) τ_i has contributions from internal modes, such as rotations about the immediate bonds that connect the nitroxide to the backbone (*14*). Figure 5 provides the plot of experimentally estimated values of $1/(\tau_{iso})$ versus $1/\eta$ (the inverse of the viscosity). The viscosity-independent tumbling time was $\tau_i = 1.52$ and the viscosity-dependent time was $\tau_R = 1.07$ ns. We discovered upon simulating the EPR spectra in Figure 4 with an axial diffusion tensor that the probe motion appeared to become progressively more anisotropic as the viscosity increased so that $\tau_{||}$ and $\tau_{\perp}$ became progressively more unequal. The inequality meant that the experimental spectra became progressively more accurately simulated by an axial diffusion tensor. As the viscosity increased from 1 to 4.8 cP, $\tau_{\perp}$ increased by over 200% from 0.79 to 1.79 ns while $\tau_{||}$ increased only by about 50% from 0.53 to 0.78 ns. Thus $\tau_{\perp}$ in this approximation reports on viscosity-sensitive motions. (Simulations for the experimental spectra having a viscosity of 4.8 cP either with isotropic or with anisotropic tumbling are shown in the Supporting Information, Figure 4S.)

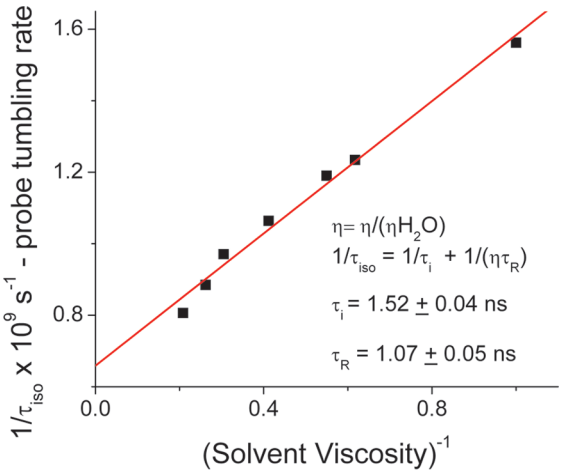

FIGURE 5: This plot of the tumbling rate ($1/\tau_{iso}$) versus the inverse of the viscosity ($1/\eta$) is used to phenomenologically separate the intrinsic tumbling, τ_i, of the spin probe from the viscosity-dependent tumbling, τ_R, of the RNA stem loop 3 to which the probe is attached.

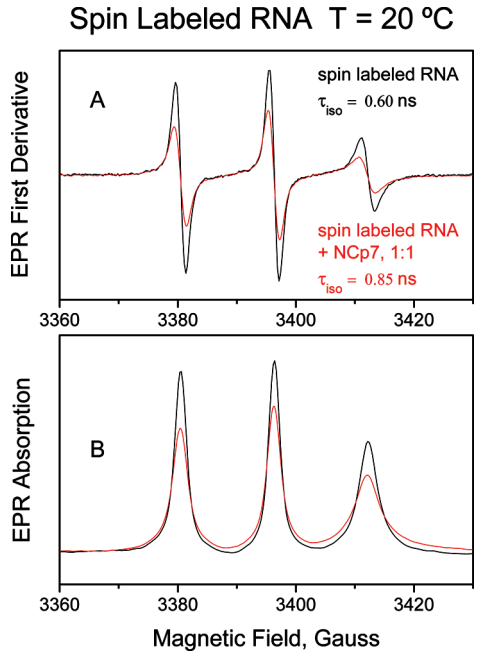

FIGURE 6: This figure compares the EPR absorption first derivative (A) and the direct absorption (B) spectra of spin-labeled RNA stem loop 3 by itself (black traces) and then with a 1:1 mixture of spin-labeled RNA stem loop 3 and NCp7 (red traces). Spectra were normalized on the second integral. These spectra were obtained at low ionic strength in 20 mM Hepes buffer, 20 mM NaCl, and 0.2 mM $MgCl_2$, pH 7.5, at 20 °C. The RNA concentration was 100 μM. For simulations of spin-labeled RNA stem loop 3 by itself see Figure 3S, Supporting Information, and for spin-labeled RNA stem loop + NCp7, 1:1, see Figure 5S, Supporting Information.

Immobilization of Spin-Labeled RNA Stem Loop 3 by NCp7: Importance of the NCp7/RNA Ratio. Next we probed the change in spin dynamics resulting from binding of RNA stem loop 3 to NCp7. In Figure 6 both the first derivative and the integrated absorption EPR spectra from RNA stem loop 3 are compared in the absence of NCp7 to the corresponding spectra in the presence of NCp7 at a 1:1 ratio at low ionic strength. The presence of the NCp7 caused a substantial increase in the tumbling time from $\tau_{iso} = 0.60$ to 0.85 ns, and so it is clear that binding of NCp7 can alter the tumbling, even of the relatively mobile spin-label at the 5′

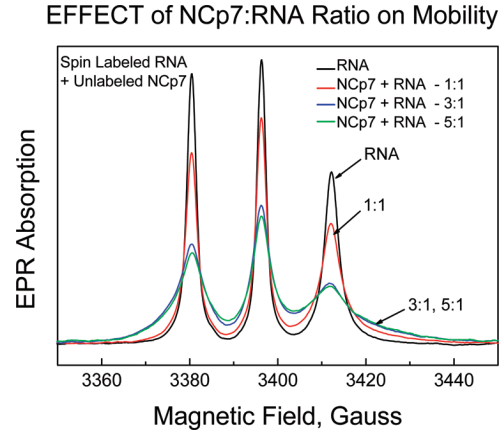

FIGURE 7: This figure compares the absorption EPR line shapes of the 5′-labeled RNA stem loop 3 at the indicated ratios of NCp7/RNA under conditions of low ionic strength. The EPR spectrum of the spin-labeled RNA by itself indicated a tumbling time τ_{iso} = 0.60 ns. The binding of NCp7 at a ratio of 1:1 slowed the tumbling to τ_{iso} = 0.85 ns. A 3:1 or 5:1 ratio of NCp7/RNA led to a significantly immobilized complex having a major, slowly tumbling component with $\tau_{iso} > 4$ ns. Spectra were normalized on the second integral. Sample conditions: 20 mM Hepes, 20 mM NaCl, and 0.2 mM $MgCl_2$, pH 7.5. Simulations of NCp7 + spin-labeled RNA, 3:1, at 20 °C are provided in Figure 6S, Supporting Information. The RNA concentration was 100 μM.

terminal. The EPR line shape in dilute buffer for the 1:1 complex was well simulated with an isotropic diffusion tensor, and the simulation of the 1:1 complex is compared with the experimental spectrum in Figure 5S, Supporting Information.

NCp7 performs some of its biological functions (*35, 36*) at ratios other than the 1:1 ratio of the NMR structure of Figure 1. We followed the EPR line shape as we varied the NCp7/RNA ratio through 0:1, 1:1, 3:1, to 5:1 in buffer of low ionic strength. As best shown by the integrated EPR spectral presentations of Figure 7, a 3:1 or 5:1 ratio of NCp7 to RNA stem loop 3 brought on a marked spectral broadening, which strongly indicated a much more immobilized NCp7/RNA stem loop 3 complex than at 0:1 and 1:1. Previous NCp7/RNA binding studies have indicated that one NCp7 can cover 6−8 RNA bases (*37*−*39*), and a 3:1 ratio of NCp7 to RNA stem loop 3 provides approximately that ratio of NCp7 to RNA bases. It will be noted that at such a ratio the +9 charge (*40*) of the NCp7 more than compensates for the −20 charge of the RNA. In the course of determining via UV−vis if thermal melting of RNA stem loop 3 was altered by the presence of NCp7, we discovered significant light scattering when the ratio of NCP7 to RNA was ≥3 under conditions of low ionic strength. This scattering occurred at wavelengths of 260 nm and higher and implied the existence of NCp7/RNA coaggregates whose size was of the order of the wavelength.

When the EPR spectra of the immobilized 3:1 NCp7/RNA complex at low ionic strength at both 5 and 20 °C (and also the 5:1 complex at 20 °C) were fit to a diffusion tensor using the NLSL routine (*32*), we noted that a much better fit was obtained if one included two spectral components, each having a different τ_{iso} tumbling time. A comparison of the experimental data to a simulation with two different isotropic tumbling times and to a simulation with one component is shown for 20 °C in Figure 6S in the Supporting Information and for 5 °C in Figure 7S. There was a majority ∼60%

component having $\tau_{iso} > 4$ ns at 20 °C and $\tau_{iso} > 7$ ns at 5 °C and a faster moving minority ~40% component with $\tau_{iso} = 1.3$ ns at 20 °C and $\tau_{iso} = 1.6$ ns at 5 °C. At this time it is not clear if there are in fact two separate populations of the NCp7/RNA complex, where the spin-label motion is more attenuated in one population than in the other or whether there are two different conformations of spin-label within the same population.

The line broadening of the nitroxide M = ±1, 0 EPR features which are simulated by NLSL methods (*32*) reflects molecular tumbling that partially averages anisotropic Zeeman and hyperfine interactions. This tumbling-induced broadening is due to single nitroxide molecules and should be independent of nitroxide concentration. However, there is the potential in large, multi-RNA, multi-NCp7 complexes to have spin−spin dipolar interactions between the nitroxides on separate RNA molecules. To probe for such spin−spin dipolar broadening, we compared 1:0, 1:1, 3:1, and 5:1 NCp7/RNA complexes made with different magnetic dilutions of spin-labeled RNA. Specifically, as shown in the Supporting Information, Figure 9S, we compared the absorption EPR line shape of these complexes prepared with 100% spin-labeled RNA stem loop 3 to that of complexes prepared with a magnetically diluted 50% spin-labeled RNA-50% unlabeled RNA mixture. In the 3:1 and 5:1 complexes the line broadening appears essentially independent of magnetic dilution, but close observation showed a barely detectable line broadening of features from the sample prepared with the more magnetically concentrated, 100% spin-labeled RNA.[2]

Immobilization of Spin-Labeled RNA Stem Loop 3 by NCp7: Importance of the Ionic Interaction between NCp7 and RNA Stem Loop 3. At a higher ionic strength due to 200 or 500 mM NaCl, the mobility of the spin-label when the NCp7/RNA ratio was kept at 3:1 was significantly increased over that in low ionic strength; this increasing mobility is shown in Figure 8 by the narrower EPR line shapes. The tumbling time in the presence of 200 mM NaCl was approximately that of the 1:1 NCp7 RNA stem loop 3 complex, while the tumbling time in the presence of 500 mM NaCl was nearly as small as that of spin-labeled RNA by itself.

Immobilization of Spin-Labeled RNA Stem Loop 3 by NCp7: Importance of Zn Fingers. As determined here by spin-label study, the interaction of NCp7 and RNA stem loop 3 at a 3:1 ratio was not purely of ionic nature. The presence of intact Zn fingers markedly enhanced the immobilization of the 5′ spin-label. Figure 9C taken at 5 °C showed the expected evidence for immobilization of the 3:1 NCp7/RNA complex at low ionic strength for a holo-NCp7 having intact Zn fingers. There was a large gain in probe mobility, as indicated in Figure 9B, that occurred for an apo-NCp7

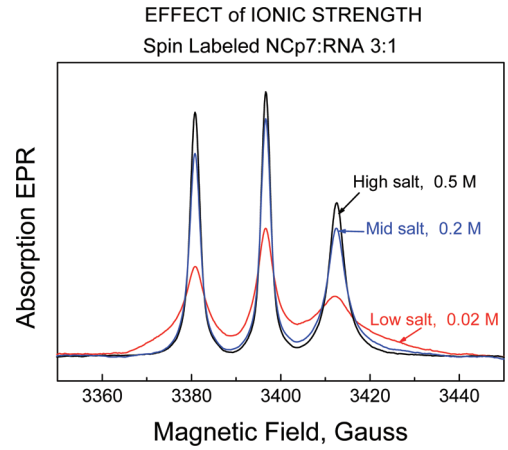

FIGURE 8: This figure compares the integrated line shapes of the 5′-labeled RNA stem loop 3 when there was a 3:1 ratio of NCp7/RNA under conditions of increasing ionic strength. The lowest concentration salt spectrum showed a major component with tumbling time greater than 3 ns. The isotropic tumbling time at 0.2 M NaCl was 0.78 ns, and the isotropic tumbling time at 0.5 M NaCl was 0.71 ns. Spectra were normalized on the second integral. The buffer conditions were 20 mM Hepes, varying NaCl, and 0.2 mM $MgCl_2$, pH = 7.5.

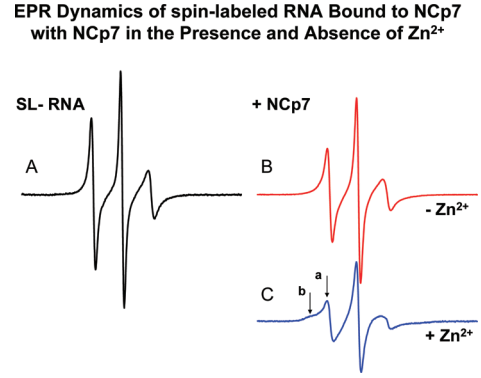

FIGURE 9: Top, left: (A) First derivative EPR spectrum of spin-labeled RNA stem loop 3 ($\tau_{iso} = 1.0$ ns). Top, right: (B) EPR spectrum upon addition of a 3× excess of apo-NCp7 without zinc ($\tau_{iso} = 1.4$ ns). Bottom, right: (C) EPR spectrum upon addition of a 3× excess of holo-NCp7 with zinc ($\tau_{iso} = 1.6$ ns for feature a, which accounts for 42% of the spins, and $\tau_{iso} = 7.4$ ns for feature b, which accounts for 58% of the spins). Temperature = 5 °C, 50 mM Hepes (low ionic strength conditions), pH 7.5. Simulations of holo-NCp7 + spin-labeled RNA, 3:1, at 5 °C are provided in Figure 7S, Supporting Information. An overlay of the experimental holo-NCp7 + spin-labeled RNA, 3:1, at 5 °C and the experimental apo-NCp7 + spin-labeled RNA, 3:1, at 5 °C is provided in Figure 8S, Supporting Information.

lacking Zn^{2+}. (An overlaid comparison of both the derivative and integral EPR absorption spectra from the 3:1 complex of NCp7/RNA in the presence and absence of Zn^{2+} is provided in Figure 8S of the Supporting Information.) On comparison to the spectrum of spin-labeled RNA stem loop 3 in the absence of NCp7 (Figure 9A), the RNA in the presence of apo-NCp7 did show additional immobilization, implying that an apo-NCp7-RNA interaction of likely ionic origin under the ionic strength conditions used here does remain to slow the tumbling of the spin-label on the RNA stem loop 3, even if the Zn fingers are not intact.

Kinetics of the Immobilization of Spin-Labeled RNA Stem Loop 3 by NCp7: Stopped-Flow EPR. The previous EPR spectra show equilibrium evidence for interaction of NCp7 with spin-labeled RNA stem loop 3. To obtain direct kinetic

[2] For the 100% spin-labeled RNA in the 3:1 and 5:1 NCp7/RNA complexes the central (M = 0) EPR feature was about 1 G broader (out of a 5 G peak width at half-height), and the outlying wings of the M = ±1 features were marginally broader than the corresponding features of the sample prepared with 50% spin-labeled RNA and 50% unlabeled. Such differential broadening may indicate the 3:1 and 5:1 complexes are multi-NCp7, multi-RNA complexes with the nitroxides of the RNA just close enough to interact by dipolar coupling. The internitroxide distance where such couplings are just detectable by liquid phase CW EPR is about 14 Å (*23*); pulsed EPR methods on frozen samples are used to detect internitroxide distances (*57*).

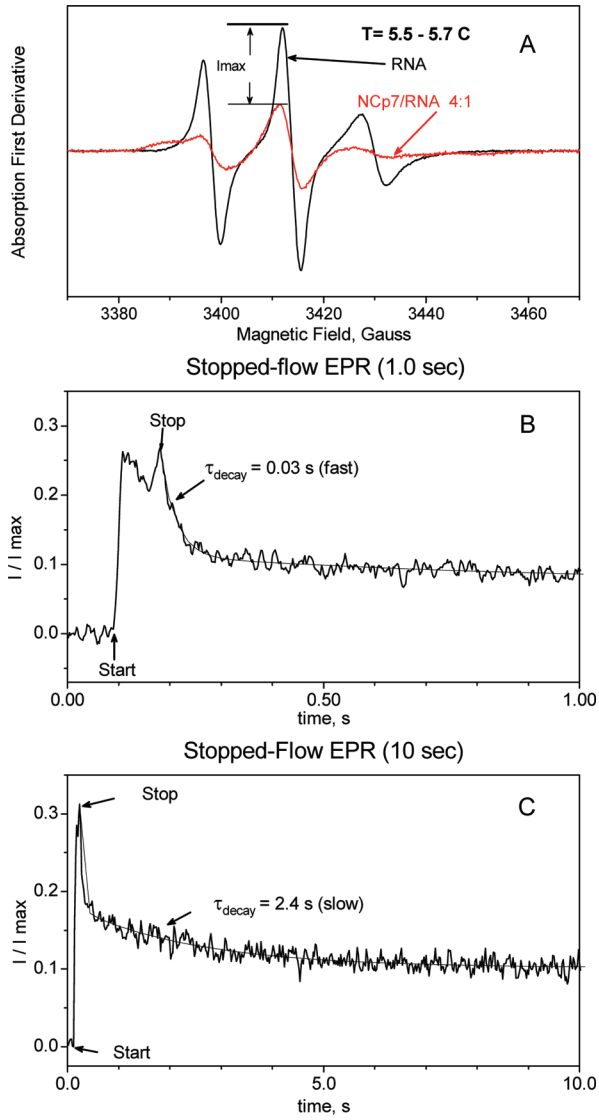

FIGURE 10: These traces show by stopped-flow EPR the interaction of NCp7 with spin-labeled RNA stem loop 3 at a 4:1 ratio as measured at 5 °C. Trace A compares the derivative EPR signal of the spin-labeled RNA by itself to the spin-labeled RNA in the presence of 4:1 NCp7. The feature monitored kinetically is the central feature, where the difference between the spectra under equilibrium conditions is noted as I_{max}. Trace B shows the rapid decay in probe immobilization on the 30 ms time scale. It should be noted that about 75% of the EPR signal decrease due to NCp7/RNA immobilization had already occurred within the 4 ms dead time of the apparatus. There is a slower immobilization which occurs with a time constant of 2.4 s, as shown in trace C. The remaining 10% immobilization occurs over several hundred seconds.

information rather than equilibrium information for the time course of immobilization, we used our specialized micromixer stopped-flow EPR system (*21, 28*) having a ~4 ms dead time. NCp7 and RNA stem loop 3 were mixed in a 4:1 ratio which, under final, long-time equilibrium conditions, leads to a complex with high probe immobilization. Figure 10A shows equilibrium EPR evidence for the considerable immobilization of the spin probe that occurs. The change in the amplitude of the central feature was followed kinetically; the difference in intensity of this central feature between spin-labeled RNA by itself and spin-labeled RNA at equilibrium in the presence of 4:1 NCp7 is denoted as I_{max}. First, it is important to point out that there was a sub-4 ms burst phase occurring within the dead time of the mixer that accounted for ~75% of the overall EPR signal change, implying that much of the interaction and recognition between RNA stem loop 3 and NCp7 occurred faster than 4 ms. Then the stopped-flow trace of Figure 10B indicated a fast transient of probe immobilization with a ~30 ms decay time. There was a slower subsequent 2.4 s transient shown in the trace of Figure 10C. The remaining immobilization, accounting for about 10% of the kinetic change, occurred over several hundred seconds. The detailed significance of these kinetic events, consistent with initial rapid NCp7/RNA binding followed by a slower complex forming process, is discussed below.

DISCUSSION

Motion of the 5′ Spin-Label on RNA Stem Loop 3 by Itself. The 5′ spin-label was end-positioned to avoid interfering with the integrity of the stem loop and with the NCp7 binding process. It is clear (see Experimental Procedures section) that the melting temperature showing integrity of the stem was unchanged by the end label and that the comparative NCp7 binding, measured by fluorescence quenching and by gel shift assay, was not impeded by the end label. At room temperature in dilute buffer, the motion of the end label on the stem loop with no NCp7 present is faster, at $\tau_{iso} = 0.60$ ns, than the expected overall tumbling rate of the 6.8 kDa stem loop. Even if the spin-labeled RNA were a 6.8 kDa sphere, rather than an approximate helix, its tumbling correlation time would be at least 1.8 ns, and this time would be longer if the anisotropic shape of the RNA is considered.[3] As shown by the dependence of the tumbling rate, $1/\tau_{iso}$, on viscosity (Figure 5 and eq 1), the spin-label had viscosity-independent local motion with a diffusion time, $\tau_i = 1.52$ ns, and viscosity-dependent motion with a diffusion time, $\tau_R = 1.07$ ns. $\tau_R = 1.07$ ns was about 60% of the 1.8 ns time estimated for overall RNA tumbling as a 6.8 kDa sphere and about 40% of the average 2.6 ns tumbling time of the RNA taken as an approximate helix.[4] Thus, τ_R is empirically equal to the tumbling time of a significant fraction of the stem loop RNA. We interpret the latter viscosity-dependent motions as a combination of fraying of the RNA duplex near its 5′ end and of overall RNA tumbling and the viscosity-independent local motion, τ_i, as motion of the probe on its immediate tether to the RNA.

Motion of the 5′ Spin-Label on RNA Stem Loop 3 When Complexed with NCp7 at a 1:1 Ratio. The complex studied here by EPR is likely to be similar to the 1:1 NCp7/RNA

[3] A 6.8 kDa rigid sphere should tumble with ~1.8 ns correlation time at room temperature in dilute buffer ($\eta \approx 1$ cP) (see formula 5 of Qin et al. (*14*)), where for a sphere the tumbling time is proportional to the molecular weight. If one takes the RNA from Figure 1 as approximating a helix with a 16.5 Å diameter and a 38 Å length, then according to the theory of Tirado and de la Rorre (their eqs 44 and 50 (*63*)), one expects $\tau_{||} = 1.6$ ns and $\tau_{\perp} = 4.2$ ns, from which an approximate τ_{iso} would be $\tau_{iso} \approx (\tau_{\perp}\tau_{||})^{1/2} = 2.6$ ns (*14*).

[4] As noted in the Results section, we determined that, upon simulating EPR spectra of Figure 4 with an axial diffusion tensor, the simulation to the spectra became better with progressively more anisotropic character as the viscosity increased. The majority of the viscosity dependence was in $\tau_{\perp}$. The implication is that $\tau_{||}$ largely represents the fast, intrinsic, viscosity-independent local motion of the probe about its immediate tethering bonds, while $\tau_{\perp}$ largely represents the slower viscosity-dependent component of the RNA stem loop diffusive motion in the perpendicular direction. The expression $\tau_{iso} \approx (\tau_{\perp}\tau_{||})^{1/2}$ would provide an approximate composite of the two motions.

stem loop 3 complex whose structure was obtained by NMR (*1*) at about an order of magnitude higher RNA and NCp7 concentrations and in a solution of about double the ionic strength we used. Presence of NCp7 at a 1:1 ratio increased the tumbling time, τ_{iso}, by 40% from 0.60 to 0.85 ns in dilute buffer. As discussed just above, the τ_R component of τ_{iso} measures the viscosity-dependent tumbling of a substantial fraction of the volume of RNA stem loop 3. If we assume that this volume is increased by binding of NCp7, τ_R would likewise be increased. Specifically, by using eq 1 and assuming that τ_i remains unchanged, one finds that the binding of one NCp7 to one RNA stem loop 3 would increase τ_R by 82% from 1.07 to 1.95 ns. Such an increase in τ_R could be construed as an 82% increase in the tumbling volume sensed by the spin probe.

Motion of the 5′ Spin-Label on RNA Stem Loop 3 in NCp7/RNA Complexes with NCp7/RNA ≥ 3. At a 3:1 NCp7 to RNA stem loop 3 ratio under conditions of low ionic strength, a marked line width increase occurred, as shown in Figure 7. A 3:1 ratio of NCp7 to 20-mer RNA stem loop 3 represents a nucleotide (nt) to NCp7 ratio of 6.7. Under these conditions the NCp7/RNA complex has a structure which caused immobilization even of the previously mobile 5′ end label.[5] The broad EPR line width, evidencing an NCp7/RNA complex which immobilizes the 5′ label, was eliminated by higher salt, as shown in Figure 8. This finding is consistent with a salt-induced electrostatic shielding that reduces the electrostatic component of the RNA-NCp7 polyanion−polycation interaction. However, NCp7 is not just a polycation; it has structured Zn-finger regions. When zinc was eliminated, the evidence for strong immobilization of the RNA disappeared, as shown by the comparison of the narrower line shape in Figure 9B where the NCp7 had no Zn^{2+} to the broader line shape of Figure 9C where NCp7 had Zn^{2+}. Since the Zn-finger region of NCp7 specifically interacts with the loop region of the RNA (*1*), there must be a specific Zn-finger-dependent component to the NCp7/induced formation of large complexes. Our EPR kinetic study (Figure 10) demonstrated the concomitant kinetics with a rapid burst of immobilization occurring within the 4 ms dead time of the apparatus, followed by a fairly rapid ∼30 ms process, and then slower diminishment of the EPR signal over a time of seconds and longer as the spin probe became progressively more immobilized.

From the foregoing measurements on EPR line shape, on ionic strength dependence, on the effect of intact Zn fingers in the NCp7, and on the kinetic immobilization behavior, we concluded that a larger complex than the 1:1 NCp7/RNA complex was being formed when NCp7/RNA ≥ 3. We address important questions regarding the formation of this larger NCp7/RNA complex: (1) Has the phenomenon been see before? (2) What is its relevance to biological function? (3) What is its basis in polymer theory? (4) What does the spin probe report?

Where Has the Formation of Larger Complexes and Coaggregates of NCp7 with Oligonucleotides Been Previously Observed? Coaggregation of NCp7 and polynucleotides has previously been reported for both long single strand oligonucleotides (*37*−*39*) and oligonucleotides as small as single strand 24-mer DNA (*41*). The ratio NCp7 per nucleotide in these studies was sufficient to cover the oligonucleotide and was in the range of 6−8 nucleotides/NCp7; the phenomenon was enhanced by low ionic strength. The aggregating aspect of the NCp7-oligonucleotide interaction appears to require the basic N-terminal tail of 1−55 NCp7 used here, whereas shorter 12−55 NCp7 lacking that tail will bind to loop regions but lacks the aggregating propensity (*42*). As determined by surface plasmon resonance, NCp7 does bind specifically and strongly to loop regions of DNA and RNA, but there is additional evidence for more weakly bound NCp7 molecules (*43*) whose presence would lead to NCp7 coverage of the RNA. Other complexes with more protein than RNA are discussed by Fisher et al. (*44*) and Hagen and Fabris (*45*).

How Does the Aggregating Function of NCp7 Correlate with Biological Functions? The relevant biological functions are to chaperone the formation of duplex RNA-DNA or DNA-DNA structures during genome replication and to cover the viral genome to protect it from unwanted nuclease attack during genome packaging. In the chaperone process nucleotide loops are recognized, stem loop structures destabilized, and duplex structures, if there should be cDNA and RNA strands available, annealed. There is a threshold concentration required for demonstrable nucleic acid chaperone effects (*7*); it is generally in the range of 7 nucleotides per NCp7 (*7*). This is the range over which the nucleic acids are almost completely covered with NCp7 (*46*−*50*). The maximum annealing rate requires more NCp7 molecules than just those needed for high affinity specific NCp7 binding to loops (*51*). The low ionic strength conditions which we use here on the small model RNA stem loop 3/NCp7 system are very similar to those of the *in vitro* annealing assay (*52*) in which complementary TAR RNA and TAR DNA secondary stem loop structures are destabilized by coverage with NCp7 and then converted to duplex RNA-DNA structures. These annealing assays were done with oligonucleotide and NcCp7 reactants in the submicromolar range (*52*), and even then there was evidence of NCp7-oligonucletide aggregation. The RNA-condensing-packaging function of the nucleocapsid complex with the entire viral genome *in vivo* (*53*) at physiological ionic strength (∼150 mM) is considerably more complex than NCp7 binding here to the model RNA stem loop 3. *In vivo* the initial selection of stem loop regions is probably highly specific and 1:1 with several loops being involved with multiple nucleocapsid domains. Interaction of the genome with more nucleocapsid domains leads to mature RNA/NCp7 complexes where the genomic RNA is coated in a nonstoichiometric manner every 6−8 nucleotides by NCp7. When the slowly tumbling complex formation occurs here for the RNA stem loop 3/NCp7 complex, there are 6−8 nucleotides per NCp7.

What Is the Polymer Theory Basis of the Immobilization? Theory developed by Bloomfield indicates that polyanionic oligonucleotides are susceptible to condensation by polyca-

[5] It is possible that the ∼40% fraction of spins with $\tau_{iso} = 1.3$ ns could arise if the fast intrinsic motion of the probe, τ_i, were retained but τ_R were increased by multiple NCp7 binding. This would mean that the viscosity-dependent motions (overall tumbling and fraying) would be slowed for RNA bound to several NCp7. If one uses eq 1 and assumes that $\tau_i = 1.57$ ns remains unchanged, τ_R would have a value of ∼9 ns to account for $\tau_{iso} = 1.3$ ns. Nine nanoseconds is the tumbling time of roughly a 30 kDa globular complex. Thus it is conceivable to have the local motion (τ_i) of the probe retained while the probe is partially immobilized in a large complex (τ_R long) so that τ_{iso} still stays fairly short (∼1.3 ns).

Table 1: 5′-Labeled RNA Stem Loop 3: Tumbling Dynamics

sample conditions	temp (°C)	τ_{iso}[a] (ns)
RNA by itself (20 mM Hepes, 20 mM NaCl, 0.2 mM $MgCl_2$, pH 7.5)	20	0.60 ± 0.05
RNA by itself (20 mM Hepes, 20 mM NaCl, 0.2 mM $MgCl_2$, pH 7.5, high viscosity, η = 4.8 cP)	20	1.24 ± 0.10[b]
RNA by itself (50 mM Hepes, pH 7.5)	5	1.1 ± 0.10
NCp7-RNA, 1:1 (20 mM Hepes, 20 mM NaCl, 0.2 mM $MgCl_2$, pH 7.5), low ionic strength	20	0.85 ± 0.07
NCp7-RNA, 3:1 (20 mM Hepes, 20 mM NaCl, 0.2 mM $MgCl_2$, pH 7.5), low ionic strength	20	5.3 ± 0.6 (58%),[c] 1.3 ± 0.07 (42%)[c]
NCp7-RNA, 5:1 (20 mM Hepes, 20 mM NaCl, 0.2 mM $MgCl_2$, pH 7.5), low ionic strength	20	4.4 ± 0.6 (63%),[c] 1.3 ± 0.07 (37%)[c]
NCp7-RNA, 3:1 (20 mM Hepes, 200 mM NaCl, 0.2 mM $MgCl_2$, pH 7.5), intermediate ionic strength	20	0.78 ± 0.08
NCp7-RNA, 3:1 (20 mM Hepes, 500 mM NaCl, 0.2 mM $MgCl_2$, pH 7.5), high ionic strength	20	0.71 ± 0.08
NCp7-RNA, 3:1 (50 mM Hepes, pH 7.5), low ionic strength, no Zn^{2+}	5	1.4 ± 0.10
NCp7-RNA, 3:1 (50 mM Hepes, pH 7.5), low ionic strength, with Zn^{2+}	5	7.1 ± 0.7 (58%),[c] 1.6 ± 0.2 (42%)[c]

[a] By estimate from nonlinear least-squares stochastic Liouville fit of the EPR spectrum (NLSL) (*32*). [b] A somewhat better fit to the tumbling of RNA by itself in viscous 0.6 g of sucrose/g of water, η = 4.8 cP, was provided by an axial diffusion tensor with $\tau_\perp$ = 1.79 ns and $\tau_\parallel$ = 0.78 ns. [c] The correlation times and the percentages of both sites were varied in the nonlinear least-squares stochastic Liouville fit to obtain these numbers.

tions (*54*), and NCp7, with its excess of lysines and arginines, is definitely a polycation. Specifically, RNA stem loop 3 has a charge estimated at −19, and NCp7 has a charge estimated as +9 (*40*). When oligonucleotide polyanions are condensed by polycations, the condensation is known to have a large electrostatic component (*54*). Such an electrostatic component can be reduced by shielding of small ions. Charge balance is important in condensation, but the detailed interactions of the polycations with each other and their excluded volume effects are also important. Because of its Zn-finger region that favors binding to loops and specific oligonucleotide sequences within loops, NCp7 is in its interaction with some oligonucleotides more than just a polycation (*1, 3*). Finally, other work of Bloomfield (*55*) shows that oligonucleotide condensation exhibits a rapid millisecond recognition phase between oligonucleotide and polycation followed by much slower aggregation on the second or longer time scale.

What Is Happening to the Spin Probe and What Does It Report? The spin-label reports longer correlation times than found either in stem loop 3 by itself or with the 1:1 NCp7/RNA complex. The implication is that local motions of the probe (τ_i in eq 1) and fast fraying motions (fast contributions to τ_R in eq 1) of the RNA have been frozen out. Such motions, called segmental motions when measured by fluorescence anisotropy decay methods, were found to be frozen out during condensation of DNA by NCp7 at a ratio of 1 NCp7 to 8 bases (*37*). We found two subsets of immobilized spin-label spectra (∼60% with $\tau_{iso} > 4$ ns and ∼40% with $\tau_{iso} \sim 1.3$ ns). An explanation is that in the subset with the longer τ_{iso} the spin-label is enveloped more completely in the NCp7/RNA complex. τ_{iso} = 4.4 ns (Table 1) would correspond to the tumbling of at least a 16 kDA sphere (*3*), although the complex could certainly be larger than this sphere if there is residual probe motion within it. In the other ∼40% subset the spin-label is freer but may still be bound to a large complex (*5*). The increased mobility of the spin brought on by increased ionic strength is a sign for loss of nonspecific, ionically bound NCp7 from the NCp7/RNA complex and of diminished complex size. The need for intact zinc fingers in stabilizing the complex is indicated by the increased probe mobility in the absence of Zn^{2+}. The time course of the kinetics of stopped-flow probe immobilization in Figure 10 is highly analogous to the kinetics of oligonucleotide condensation described in the previous paragraph.

The immobilization phenomena which we have observed for the 20-mer stem loop 3 RNA at ratios of NCp7 to oligonucleotide which cover the oligonucleotide need not be unique to this specific RNA stem loop 3, and in fact, study in progress on the stem loop 27-mer TAR DNA, labeled in both stem and loop, has revealed comparable probe immobilization brought on by NCp7. (TAR DNA has been a subject of detailed NCp7 annealing assays (*52, 56*).) One wants to understand better the structure of the condensate and interactions of NCp7 and the stem loop oligonucleotides within it. Better elucidation of the structure(s) of immobilized NCp7-oligonucleotide complexes will require spin probes in stem and loop regions and spin-labeled NCp7. The purpose of such spin probes on the stem loop oligonucleotides or on the NCp7 will be as individual probes to probe local motion and as bilabels to probe distances and distance changes between subunits of the complex (*13, 18−20, 57*).

CONCLUSIONS

With spin-labeling at a nonperturbing 5′ RNA end site, this study showed a subnanosecond probe mobility due to a combination of viscosity-dependent tumbling and fraying and viscosity-independent local probe motion. The binding of NCp7 in a 1:1 ratio to the RNA was reported by a partial, ∼40%, further immobilization (i.e., increase in tumbling correlation time) of the spin probe. This NCp7-dependent immobilization was consistent with slowing of the viscosity-dependent motion as brought on by adhesion of NCp7 to the RNA. When the ratio of NCp7 to stem loop RNA was ≥3, the tumbling time reported by the spin-label markedly increased (to >4 ns) in low ionic strength solution. The increase implied formation of a larger complex or condensate that immobilized even the end-site spin-label. By raising the ionic strength (through increased NaCl concentration) at this 3:1 ratio of NCp7 to stem loop RNA, the correlation time of the spin-label was decreased approximately to the value which it previously had at a 1:1 ratio of RNA and NCp7. The implication of the decrease was that there is an interaction between polyanionic RNA and polycationic NCp7, which can be reduced by shielding of small salt ions, and this ionic interaction was significant in increasing the adherence of NCp7 and RNA in the larger complex that immobilized the spin-label. The presence of intact Zn fingers was also critical for generating the larger complex or condensate, signifying the importance of the Zn-finger structure of NCp7, rather than simply the polycation character of NCp7, in generating the larger complex or condensate. The EPR stopped-flow kinetics of spin probe immobilization showed fast, millisecond immobilization processes followed

by a slower process on the order of seconds, and these kinetics were a sign of fast binding of RNA and NCp7 followed by condensation.

A study of local motion and tumbling at numerous backbone sites of 12−53 NCp7 and its 1:1 complex with a small DNA oligomer has been carried out by ^{15}N NMR and W37 fluorescence (*58*). However, a strong point of EPR is its facility to probe the structure and local mobility within noncrystallizeable complexes and complexes not amenable to high resolution NMR. Such complexes include those associated with fibrils in neurodegenerative Parkinson's (*59, 60*) and Alzheimer's (*61*) diseases. The EPR results reported here indicate that the spectra of the 5′ RNA end spin-label can probe the local mobility RNA in a large complex that arises under low ionic strength and at ratios of NCp7 to 20-mer RNA stem loop 3 ≥3. For our 20-mer RNA the 3:1 ratio of NCp7/RNA where EPR line broadening sets in corresponds to a coverage of 6−8 nt per NCp7. NCp7 performs here an RNA condensing role in an apparent nonstoichiometric manner, although the *in vitro* condensation of the model 20-mer RNA stem loop with NCp7 must be considerably simpler in its development than the *in vivo* condensation of genomic RNA *in vivo* to a final 6−8 nt per NCp7. These EPR results provide both the nanosecond correlation times of the spin probe mobility and the kinetic behavior on the millisecond and longer time scale for the mobility to change. This work points us in the future direction of applying spin-label EPR to detect the interaction of NCp7 and stem loop nucleotides at numerous locations and to obtain detailed structural distance information within nonstoichiometric complexes by use of simultaneous probes on RNA and NCp7. Future work, using flow EPR with submillisecond time resolution (*22, 23, 28*), will be used to probe for submillisecond fast recognition.

ACKNOWLEDGMENT

We are grateful to Prof. Keith Earle, University at Albany, for guiding us in dealing with the nonlinear least-squares stochastic Liouville (NLSL) simulations; to Prof. Carla Theimer, University at Albany, for aid in RNA PAGE purification and RNA melting; to Dr. Burckhard Seelig, Harvard Medical School, Molecular Biology and CCIB, for MALDI mass spectrometry measurements; to Dr. Edmund Howard, Department of Biochemistry, Molecular Biology, and Biophysics, University of Minnesota, for simulations using the MOMD model; to Dr. My-Nuong Vo, Department of Chemistry, University of Minnesota, for insight into annealing activity assays; and to Prof. David Thomas, Department of Biochemistry, Molecular Biology, and Biophysics, University of Minnesota, for detailed guidance.

SUPPORTING INFORMATION AVAILABLE

Figure 1S, MALDI spectra of RNA stem loop 3; Figure 2S, the fluorescence quenching of W37 in NCp7; Figure 3S, comparison of the experimental EPR and simulated spectra of spin-labeled RNA stem loop 3 by itself in dilute buffer at 20 °C; Figure 4S, comparison of experimental and simulated spectra for isotropic and axial diffusion of spin-labeled RNA stem loop 3 in a viscous buffer; Figure 5S, comparison of the experimental and simulated EPR spectra of NCp7 + spin-labeled RNA stem loop 3, 1:1, in dilute buffer at 20 °C; Figure 6S, NCp7 + spin-labeled RNA, 3:1, low ionic strength, $T = 20$ °C, comparison of experimental spectra and simulated spectra for two subsites versus one site; Figure 7S, NCp7 + spin-labeled RNA, 3:1, low ionic strength, $T = 5$ °C, comparison of experimental spectra and simulated spectra for two subsites versus one site; Figure 8S, NCp7 + spin-labeled RNA, 3:1, low ionic strength, $T = 5$ °C, comparison of the effect of NCp7 with and without Zn^{2+}; Figure 9S, compares EPR spectra of 0:1, 1:1, 3:1, and 5:1 NCp7/RNA stem loop 3 samples in which the RNA was 100% spin-labeled versus magnetically diluted to 50% spin-labeled/50% unlabeled. Protocols for preparative and analytical PAGE gel electrophoresis of RNA stem loop 3 are provided. This material is available free of charge via the Internet at http://pubs.acs.org.

REFERENCES

1. De Guzman, R. N., Wu, Z. R., Stalling, C. C., Pappalardo, L., Borer, P. N., and Summers, M. F. (1998) Structure of the HIV-1 nucleocapsid protein bound to the SL3 psi-RNA recognition element. *Science 279*, 384–388.
2. Vuilleumier, C., Bombarda, E., Morellet, N., Gerard, D., Roques, B. P., and Mély, Y. (1999) Nucleic acid sequence discrimination by the HIV-1 nucleocapsid protein NCp7: a fluorescence study. *Biochemistry 38*, 16816–16825.
3. Amarasinghe, G. K., De Guzman, R. N., Turner, R. B., Chancellor, K. J., Wu, Z. R., and Summers, M. F. (2000) NMR structure of the HIV-1 nucleocapsid protein bound to stem-loop SL2 of the psi-RNA packaging signal. Implications for genome recognition. *J. Mol. Biol. 301*, 491–511.
4. Amarasinghe, G. K., Zhou, J., Miskimon, M., Chancellor, K. J., McDonald, J. A., Matthews, A. G., Miller, R. R., Rouse, M. D., and Summers, M. F. (2001) Stem-loop SL4 of the HIV-1 psi RNA packaging signal exhibits weak affinity for the nucleocapsid protein. Structural studies and implications for genome recognition. *J. Mol. Biol. 314*, 961–970.
5. Pappalardo, L., Kerwood, D. J., Pelczer, I., and Borer, P. N. (1998) Three-dimensional folding of an RNA hairpin required for packaging HIV-1. *J. Mol. Biol. 282*, 801–818.
6. Summers, M. F., Henderson, L. E., Chance, M. R., Bess, J. W., Jr., South, T. L., Blake, P. R., Sagi, I., Perez-Alvarado, G., Sowder, R. C., III, Hare, D. R., et al. (1992) Nucleocapsid zinc fingers detected in retroviruses: EXAFS studies of intact viruses and the solution-state structure of the nucleocapsid protein from HIV-1. *Protein Sci. 1*, 563–574.
7. Rein, A., Henderson, L. E., and Levin, J. G. (1998) Nucleic-acid-chaperone activity of retroviral nucleocapsid proteins: significance for viral replication. *Trends Biochem. Sci. 23*, 297–301.
8. Macosko, J. C., Pio, M. S., Tinoco, I., Jr., and Shin, Y. K. (1999) A novel 5 displacement spin-labeling technique for electron paramagnetic resonance spectroscopy of RNA. *RNA 5*, 1158–1166.
9. Price, E. A., Sutch, B. T., Cai, Q., Qin, P. Z., and Haworth, I. S. (2007) Computation of nitroxide-nitroxide distances in spin-labeled DNA duplexes, Biopolymers.
10. Ramos, A., and Varani, G. (1998) A New Method to Detect Long-Range Protein-RNA Contacts: NMR Detection of Electron-Proton Relaxation Induced by Nitroxide Spin-Labeled RNA. *J. Am. Chem. Soc. 120*, 10992–10993.
11. Edwards, T. E., Okonogi, T. M., Robinson, B. H., and Sigurdsson, S. T. (2001) Site-specific incorporation of nitroxide spin-labels into internal sites of the TAR RNA; structure-dependent dynamics of RNA by EPR spectroscopy. *J. Am. Chem. Soc. 123*, 1527–1528.
12. Qin, P. Z., Hideg, K., Feigon, J., and Hubbell, W. L. (2003) Monitoring RNA base structure and dynamics using site-directed spin-labeling. *Biochemistry 42*, 6772–6783.
13. Qin, P. Z., and Dieckmann, T. (2004) Application of NMR and EPR methods to the study of RNA. *Curr. Opin. Struct. Biol. 14*, 350–359.
14. Qin, P. Z., Butcher, S. E., Feigon, J., and Hubbell, W. L. (2001) Quantitative analysis of the isolated GAAA tetraloop/receptor interaction in solution: a site-directed spin-labeling study. *Biochemistry 40*, 6929–6936.
15. Qin, P. Z., Feigon, J., and Hubbell, W. L. (2005) Site-directed spin-labeling studies reveal solution conformational changes in a

GAAA tetraloop receptor upon Mg(2+)-dependent docking of a GAAA tetraloop. *J. Mol. Biol. 351*, 1–8.
16. Edwards, T. E., and Sigurdsson, S. T. (2002) Electron paramagnetic resonance dynamic signatures of TAR RNA-small molecule complexes provide insight into RNA structure and recognition. *Biochemistry 41*, 14843–14847.
17. Edwards, T. E., Robinson, B. H., and Sigurdsson, S. T. (2005) Identification of amino acids that promote specific and rigid TAR RNA-tat protein complex formation. *Chem. Biol. 12*, 329–337.
18. Schiemann, O., Weber, A., Edwards, T. E., Prisner, T. F., and Sigurdsson, S. T. (2003) Nanometer distance measurements on RNA using PELDOR. *J. Am. Chem. Soc. 125*, 3434–3435.
19. Kim, N. K., Murali, A., and DeRose, V. J. (2004) A distance ruler for RNA using EPR and site-directed spin labeling. *Chem. Biol. 11*, 939–948.
20. Cai, Q., Kusnetzow, A. K., Hideg, K., Price, E., Haworth, I. S., and Qin, P. Z. (2007) Nanometer distance measurements in RNA using site-directed spin labeling, Biophys. J.
21. Grigoryants, V. M., Veselov, A. V., and Scholes, C. P. (2000) Variable velocity liquid flow EPR applied to submillisecond protein folding. *Biophys. J. 78*, 2702–2708.
22. DeWeerd, K., Grigoryants, V., Sun, Y., Fetrow, J. S., and Scholes, C. P. (2001) EPR-detected folding kinetics of externally located cysteine-directed spin-labeled mutants of Iso-1-cytochrome c. *Biochemistry 40*, 15846–15855.
23. Grigoryants, V. M., DeWeerd, K. A., and Scholes, C. P. (2004) Method of rapid mix EPR applied to the folding of bi-spin-labeled protein as a probe for the dynamic onset of interaction between sequentially distant side chains. *J. Phys. Chem. B 108*, 9463–9468.
24. Karim, C. B., Zhang, Z., and Thomas, D. D. (2007) Synthesis of TOAC spin-labeled proteins and reconstitution in lipid membranes. *Nat. Protoc. 2*, 42–49.
25. Karim, C. B., Zhang, Z., Howard, E. C., Torgersen, K. D., and Thomas, D. D. (2006) Phosphorylation-dependent conformational switch in spin-labeled phospholamban bound to SERCA. *J. Mol. Biol. 358*, 1032–1040.
26. Tummino, P. J., Scholten, J. D., Harvey, P. J., Holler, T. P., Maloney, L., Gogliotti, R., Domagala, J., and Hupe, D. (1996) The in vitro ejection of zinc from human immunodeficiency virus (HIV) type 1 nucleocapsid protein by disulfide benzamides with cellular anti-HIV activity. *Proc. Natl. Acad. Sci. U.S.A. 93*, 969–973.
27. Theimer, C. A., Wang, Y., Hoffman, D. W., Krisch, H. M., and Giedroc, D. P. (1998) Non-nearest neighbor effects on the thermodynamics of unfolding of a model mRNA pseudoknot. *J. Mol. Biol. 279*, 545–564.
28. Scholes, C. P. (2005) EPR Interfaced to Rapid Mixing, in *Biological Magnetic Resonance—Part B: Methodology, Instrumentation, and Dynamics* (Eaton, G. R., Eaton, S. S., and Berliner, L., Eds.) pp 53−88, Kluwer Academic Publishers, Norton, MA.
29. Marsh, D. (1989) in *Biological Magnetic Resonance* (Berliner, L., and Ruben, J., Eds.)Chapter 255, pp 255−303, Plenum, New York.
30. Miick, S. M., Todd, A. P., and Millhauser, G. L. (1991) Position-dependent local motions in spin-labeled analogues of a short α-helical peptide determined by electron spin resonance. *Biochemistry 30*, 9498–9503.
31. Qu, K., Vaughn, J. L., Sienkiewicz, A., Scholes, C. P., and Fetrow, J. S. (1997) Kinetics and motional dynamics of spin-labeled yeast iso-1-cytochrome c: 1. Stopped-flow electron paramagnetic resonance as a probe for protein folding/unfolding of the C-terminal helix spin-labeled at cysteine 102. *Biochemistry 36*, 2884–2897.
32. Budil, D. E., Lee, S., Saxena, S., and Freed, J. H. (1996) Nonlinear-Least-Squares Analysis of Slow-Motion EPR Spectra in One and Two Dimensions Using a Modified Levenberg-Marquardt Algorithm. *J. Magn. Reson., Ser. A 120*, 155–189.
33. Earle, K. A., and Budil, D. E. (2006) Calculating Slow-motion ESR Spectra of Spin-Labeled Polymers, in *Advanced ESR Methods in Polymer Research* (Schlick, S., Ed.)Chapter 3, John Wiley and Sons, New York.
34. Mchaourab, H. S., Lietzow, M. A., Hideg, K., and Hubbell, W. L. (1996) Motion of spin-labeled side chains in T4 lysozyme. Correlation with protein structure and dynamics. *Biochemistry 35*, 7692–7704.
35. Darlix, J. L., Lapadat-Tapolsky, M., de Rocquigny, H., and Roques, B. P. (1995) First glimpses at structure-function relationships of the nucleocapsid protein of retroviruses. *J. Mol. Biol. 254*, 523–537.
36. Tanchou, V., Gabus, C., Rogemond, V., and Darlix, J. L. (1995) Formation of stable and functional HIV-1 nucleoprotein complexes in vitro. *J. Mol. Biol. 252*, 563–571.
37. Krishnamoorthy, G., Roques, B., Darlix, J. L., and Mély, Y. (2003) DNA condensation by the nucleocapsid protein of HIV-1: a mechanism ensuring DNA protection. *Nucleic Acids Res. 31*, 5425–5432.
38. Stoylov, S. P., Vuilleumier, C., Stoylova, E., De Rocquigny, H., Roques, B. P., Gerard, D., and Mély, Y. (1997) Ordered aggregation of ribonucleic acids by the human immunodeficiency virus type 1 nucleocapsid protein. *Biopolymers 41*, 301–312.
39. Urbaneja, M. A., Kane, B. P., Johnson, D. G., Gorelick, R. J., Henderson, L. E., and Casas-Finet, J. R. (1999) Binding properties of the human immunodeficiency virus type 1 nucleocapsid protein p7 to a model RNA: elucidation of the structural determinants for function. *J. Mol. Biol. 287*, 59–75.
40. Shubsda, M. F., Paoletti, A. C., Hudson, B. S., and Borer, P. N. (2002) Affinities of packaging domain loops in HIV-1 RNA for the nucleocapsid protein. *Biochemistry 41*, 5276–5282.
41. Tsuchihashi, Z., and Brown, P. O. (1994) DNA strand exchange and selective DNA annealing promoted by the human immunodeficiency virus type 1 nucleocapsid protein. *J. Virol. 68*, 5863–5870.
42. Bernacchi, S., Stoylov, S., Piemont, E., Ficheux, D., Roques, B. P., Darlix, J. L., and Mély, Y. (2002) HIV-1 nucleocapsid protein activates transient melting of least stable parts of the secondary structure of TAR and its complementary sequence. *J. Mol. Biol. 317*, 385–399.
43. Fisher, R. J., Rein, A., Fivash, M., Urbaneja, M. A., Casas-Finet, J. R., Medaglia, M., and Henderson, L. E. (1998) Sequence-specific binding of human immunodeficiency virus type 1 nucleocapsid protein to short oligonucleotides. *J. Virol. 72*, 1902–1909.
44. Fisher, R. J., Fivash, M. J., Stephen, A. G., Hagan, N. A., Shenoy, S. R., Medaglia, M. V., Smith, L. R., Worthy, K. M., Simpson, J. T., Shoemaker, R., McNitt, K. L., Johnson, D. G., Hixson, C. V., Gorelick, R. J., Fabris, D., Henderson, L. E., and Rein, A. (2006) Complex interactions of HIV-1 nucleocapsid protein with oligonucleotides. *Nucleic Acids Res. 34*, 472–484.
45. Hagan, N., and Fabris, D. (2003) Direct mass spectrometric determination of the stoichiometry and binding affinity of the complexes between nucleocapsid protein and RNA stem-loop hairpins of the HIV-1 Psi-recognition element. *Biochemistry 42*, 10736–10745.
46. Feng, Y. X., Copeland, T. D., Henderson, L. E., Gorelick, R. J., Bosche, W. J., Levin, J. G., and Rein, A. (1996) HIV-1 nucleocapsid protein induces "maturation" of dimeric retroviral RNA in vitro. *Proc. Natl. Acad. Sci. U.S.A. 93*, 7577–7581.
47. Guo, J., Henderson, L. E., Bess, J., Kane, B., and Levin, J. G. (1997) Human immunodeficiency virus type 1 nucleocapsid protein promotes efficient strand transfer and specific viral DNA synthesis by inhibiting TAR-dependent self-priming from minus-strand strong-stop DNA. *J. Virol. 71*, 5178–5188.
48. Khan, R., and Giedroc, D. P. (1992) Recombinant human immunodeficiency virus type 1 nucleocapsid (NCp7) protein unwinds tRNA. *J. Biol. Chem. 267*, 6689–6695.
49. Wu, W., Henderson, L. E., Copeland, T. D., Gorelick, R. J., Bosche, W. J., Rein, A., and Levin, J. G. (1996) Human immunodeficiency virus type 1 nucleocapsid protein reduces reverse transcriptase pausing at a secondary structure near the murine leukemia virus polypurine tract. *J. Virol. 70*, 7132–7142.
50. You, J. C., and McHenry, C. S. (1994) Human immunodeficiency virus nucleocapsid protein accelerates strand transfer of the terminally redundant sequences involved in reverse transcription. *J. Biol. Chem. 269*, 31491–31495.
51. Rist, M. J., and Marino, J. P. (2002) Mechanism of nucleocapsid protein catalyzed structural isomerization of the dimerization initiation site of HIV-1. *Biochemistry 41*, 14762–14770.
52. Vo, M. N., Barany, G., Rouzina, I., and Musier-Forsyth, K. (2006) Mechanistic studies of mini-TAR RNA/DNA annealing in the absence and presence of HIV-1 nucleocapsid protein. *J. Mol. Biol. 363*, 244–261.
53. Turner, B. G., and Summers, M. F. (1999) Structural biology of HIV. *J. Mol. Biol. 285*, 1–32.
54. Bloomfield, V. A. (1997) DNA condensation by multivalent cations. *Biopolymers 44*, 269–282.
55. Bloomfield, V. A. (2000) Static and dynamic light scattering from aggregating particles. *Biopolymers 54*, 168–172.
56. Hong, M. K., Harbron, E. J., O'Connor, D. B., Guo, J., Barbara, P. F., Levin, J. G., and Musier-Forsyth, K. (2003) Nucleic acid conformational changes essential for HIV-1 nucleocapsid protein-mediated inhibition of self-priming in minus-strand transfer. *J. Mol. Biol. 325*, 1–10.

57. Borbat, P. P., Mchaourab, H. S., and Freed, J. H. (2002) Protein structure determination using long-distance constraints from double-quantum coherence ESR: study of T4 lysozyme. *J. Am. Chem. Soc. 124*, 5304–5314.
58. Ramboarina, S., Srividya, N., Atkinson, R. A., Morellet, N., Roques, B. P., Lefevre, J. F., Mely, Y., and Kieffer, B. (2002) Effects of temperature on the dynamic behaviour of the HIV-1 nucleocapsid NCp7 and its DNA complex. *J. Mol. Biol. 316*, 611–627.
59. Chen, M., Margittai, M., Chen, J., and Langen, R. (2007) Investigation of alpha -synuclein fibril structure by site-directed spin labeling. *J. Biol. Chem. 34*, 24790–24797.
60. Margittai, M., and Langen, R. (2006) Spin labeling analysis of amyloids and other protein aggregates. *Methods Enzymol. 413*, 122–139.
61. Hatters, D. M., Budamagunta, M. S., Voss, J. C., and Weisgraber, K. H. (2005) Modulation of apolipoprotein E structure by domain interaction: differences in lipid-bound and lipid-free forms. *J. Biol. Chem. 280*, 34288–34295.
62. Xiao, W., and Shin, Y. K. (2000) EPR Spectroscopic Ruler: the Deconvolution Method and its Applications, in *Biological Magnetic Resonance: Distance Measurements in Biological Systems by EPR* (Berliner, L. J., Eaton, G. R., and Eaton, S. S., Eds.) pp 249−276, Plenum, New York.
63. Tirado, M. M., and de la Torre (1980) Rotational dynamics of rigid symmetric top macromolecules. Application to circular cylinders. *J. Chem. Phys. 73*, 1986–1993.

BI800602E